Journal of Molecular Liquids 414 (2024) 126099

Contents lists available at ScienceDirect

Journal of Molecular Liquids

journal homepage: www.elsevier.com/locate/molliq

The role of ionic liquid additives in enhancing the tribological performance of plastic-derived oils

Md Hafizur Rahman [a,b], Soumya Sikdar [a], Prakashbhai R. Bhoi [b], Pradeep L. Menezes [a,*]

[a] Dept. of Mechanical Engineering, University of Nevada-Reno, Reno, NV 89503, USA
[b] Dept. of Mechanical Engineering, Georgia Southern University, Statesboro, GA 30458, USA

ARTICLE INFO

Keywords:
Bio-based additives
Friction
Ionic liquids
Lubrication
Plastic oils
Wear

ABSTRACT

Improper disposal of waste plastic contributes significantly to environmental pollution. A promising solution to address this issue involves converting such plastics into valuable lubricating oils. This study investigated the tribological performance of both an aromatic-lean industrial plastic oil (PO) and aromatic-rich lab-scale plastic oils (LPO) using a ball-on-disk setup. The results revealed that PO exhibited considerably higher coefficients of friction (COF) and specific wear rates compared to LPO. To enhance the lubrication performance, a bio-based ionic liquid (IL: trihexyltetradecyl phosphonium saccharinate) with an unsaturated anion was incorporated. The COF and wear rates were further reduced with an IL blend in both PO and LPO. The IL additive promoted increased film thickness, beneficial micelle formation, facilitated adsorption film formation, and provided a phosphorus-rich tribofilm. These mechanisms collectively contributed to the notable improvement in tribological performance. Overall, this research demonstrates the potential of IL additives to enhance the tribological performance of both PO and LPO, thereby mitigating waste plastic pollution, and fostering a sustainable future.

1. Introduction

Plastics have become a pervasive component of the modern economy, offering unique functional properties at a low cost. In 1964, the global production of plastic stood at a mere 15 million metric tons, and surged to an astonishing amount of 360 million metric tons in 2018 alone [1,2]. The significant expansion is demonstrated by the cumulative production of around 8660 million metric tons of virgin plastics up to the year 2018 [3]. The rapid increase in plastic production has resulted in a colossal waste management challenge. Amongst the produced plastic waste, only 9 % were recycled, 12 % were incinerated, and a substantial 79 % were disposed of in landfills or natural environments [3,4]. This alarming trend clearly shows the inefficacy of traditional recycling systems and imposes an urgent need to process plastic waste in alternative ways. Processing of waste plastic is also important to establish a circular plastic economy, since a lot of usable hydrocarbons are currently trapped in plastic waste. If those hydrocarbons could be utilized in the form of fuel or chemicals, that could reduce global energy demand and help establish a sustainable future for human beings on Earth. Over the past few decades, there has been a notable surge in global energy consumption, driven by factors, such as rapid population growth, the fourth industrial revolution, and the evolution of electric vehicles. A significant portion of global energy is consumed to overcome friction and wear in these machinery. It was estimated by Holmberg et al. [5] that, through novel advanced functional material research, and alternative lubrication technologies for vehicles, machinery, and other equipment; worldwide energy losses due to friction and wear could possibly be reduced by 40 % in the long term (15 years) [5]. This projection underscores the pressing need to (a) explore sustainable alternatives of traditional lubricants, and (b) incorporate innovative scientific approaches to meet the escalating demand for lubricating oil in the rapidly evolving energy landscape. Useful chemicals produced from waste plastics could play a pivotal role in meeting this energy need.

One way to treat plastic waste is to convert it into useful solid, liquid or gaseous chemicals, through thermal or thermo-catalytic pyrolysis [3,6]. The pyrolysis conversion process depends on variables such as temperatures, pressures, catalysts, and reactor types. Careful selection of these variables could help convert waste plastics into desirable liquids, in form of aromatic lean or aromatic rich hydrocarbons. Research has shown the efficacy of pyrolysis liquids to be utilized as fuels [7]. Therefore, plastic to liquid fuel production is currently in technology readiness level 6–9, meaning they are commercially available [7,8]. Although these oils have commercial demands, however, the

* Corresponding author.
E-mail address: pmenezes@unr.edu (P.L. Menezes).

https://doi.org/10.1016/j.molliq.2024.126099
Received 17 May 2024; Received in revised form 4 September 2024; Accepted 21 September 2024
Available online 24 September 2024
0167-7322/© 2024 Elsevier B.V. All rights are reserved, including those for text and data mining, AI training, and similar technologies.

Nomenclature

PO	Plastic Oil
LPO	Lab-scale Plastic Oil
LPO-A	Lab-scale Plastic Oil from 450 °C pyrolysis
LPO-B	Lab-scale Plastic Oil from 500 °C pyrolysis
LPO-C	Lab-scale Plastic Oil from 550 °C pyrolysis
HQL	High Quality Oil
RTIL	Room Temperature Ionic Liquid
HDPE	High Density Poly Ethylene
LDPE	High Density Poly Ethylene
PP	Poly Propylene
PVC	Poly Vinyl Chloride
PET	Poly Ethylene Terephthalate
ZSM-5	Zeolite Socuny Mobil-5
[P6,6,6,14][Sacc]	Trihexyltetradecylphosphonium Saccharinate
FTIR	Fourier transform infrared spectroscopy
NMR	Nuclear magnetic resonance
GC-FID	Gas Chromatography-Flame Ionization Detection
RH	Relative Humidity
CDCl3	Chloroform
TMS	Tetramethylsilane

tribological performance of such oil has received limited attention and has a research gap. A careful investigation to address this gap could open ways to utilize these plastic derived oils not only as fuels for combustion engine vehicles but also as a lubricant in electric vehicles and industrial machinery. As such, plastic derived oils can play a crucial role to reduce the friction and wear loss in moving mechanical assembly, such as engines, gearboxes, and bearings, if formulated and utilized carefully.

Recently, plastic oil (PO) tribology received researchers' attention [7]. For instance, Sikdar et al. [9] addressed the importance of PO lubrication in 2020. Later, Hackler et al. [10] compared the tribological performance of plastic derived high quality liquids (HQL) with mineral oil and found a 44 % reduction in wear for HQL compared to mineral oil. When HQL was mixed with polyalphaolefin (PAO) in 30 wt%, a 9 % reduction in friction, and a 30 % reduction in wear was achieved. Cappello et al. [11] performed the life cycle analysis (LCA) for the HQL obtained from high density polyethylene (HDPE) and observed a 74 % reduction in GHG emission for PO (0.48–1.2 kg_{CO2e} kg_{HQL}^{-1}) than traditional PAO (1.88 kg_{CO2e} kg_{Lub}^{-1}) lubricants. These studies show the evidence that plastic derived oils are competent for machine lubrication. Sikdar et al. [12] investigated the industrial POs and found that friction and wear performance of industrial PO could be enhanced upto 54 %, and 85 %, respectively by incorporating solid graphene nanoplatelets, and upto 40, and 44 % respectively by adding hexagonal boron nitride in aluminum-steel tribo-pair. While incorporating both these solid lubricant additives in a combined form improved the lubrication performance by reducing friction by 65 % and wear volume by 97 %. However, solid lubricant additive usage in mechanical systems, could offer some challenges. For instance, the solid additives can undergo sedimentation and agglomeration (in higher concentrations) that may clog fuel pipes and offer system downtime. Incorporating liquid additives can overcome these existing limitations and provide sustainable alternative lubrication solutions. One suitable liquid additive that can be utilized to enhance the lubrication performance of POs could be bio-based ionic liquids (IL) [13–16]. IL is a novel class of liquid lubricant, with favorable physicochemical and tribological properties such as high viscosity, favorable wettability, film forming ability, thermal stability [17–20]. Amongst wide possible varieties, sugar-derived aromatic ring containing saccharinate-based phosphonium IL outperformed many other ILs as reported in the literature [21,22]. Therefore, the addition of saccharinate-based phosphonium IL could enhance the lubrication performance of PO, mitigating the challenges encountered with solid lubricant additives. The physicochemical and tribological properties of IL could alter the lubrication mechanisms. The PO and IL additive blend could not only enhance the lubrication performance but also help develop an environmentally friendly, circular plastic economy for a sustainable future.

In this research, different plastic derived oils and PO-IL blends were investigated to study the tribological performances and understand their lubrication mechanisms from the chemical point of view. This research was driven by the hypothesis that the aromatic compounds in base oil and in the IL additive would significantly enhance the tribological performance of plastic-derived oils.

Table 1
Major constituents of steel specimen and the PO.

AISI 316L		PO	
Constituents	**Quantity (%)**	**Constituents**	**Quantity (%)**
C	0.023	Complex mixture of hydrocarbons	93.9
Co	0.350	n-Hexane	0.1
Cr	16.59	n-Heptane	1.5
Cu	0.360	n-Nonane	1.4
Mn	1.450	n-Decane	1.4
Mo	2.058	2,2,4-trimethylpentane	0.8
N	0.034		
Ni	10.56		
P	0.026		
S	0.021		
Fe	balance		

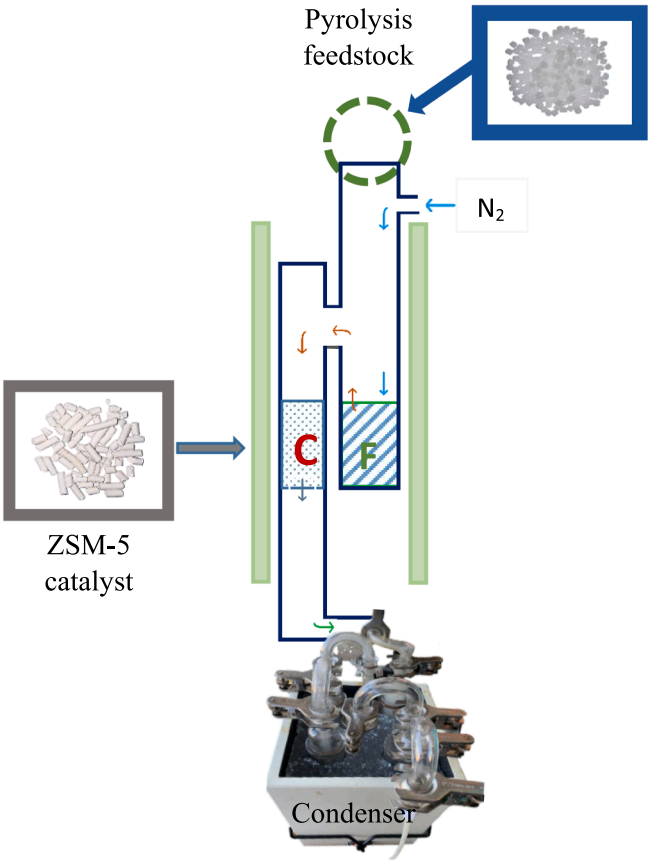

Fig. 1. Fixed bed reactor system for plastic pyrolysis. Adopted with permission from [23], Elsevier, 2021.

2. Materials and methods

In this study, two types of POs were investigated. (1) industrial PO (referred as PO) obtained from thermochemical pyrolysis of mixed plastics (HDPE, LDPE, PP, and other plastics from waste stream after separating PVC, Nylon, PET and other ingredients those hinder in oil production), and (2) laboratory-scale PO (referred as LPO) produced from thermo-catalytic pyrolysis of HDPE in a fixed bed reactor using zeolite catalyst (ZSM-5, sourced from Alfa Aeser, USA). The IL was synthesized in the laboratory. The raw materials to synthesize the IL were: trihexyl tetradecyl phosphonium chloride and sodium saccharinate salt hydrate, both procured from an external supplier (Milipore Sigma, USA). The synthesized IL: trihexyl tetradecyl phosphonium saccharinate [P6,6,6,14][Sacc] was used as an additive to PO at 1 %, 2 %, and 5 % concentrations. The lubrication performance of each concentrations of base PO (without any IL), PO-IL blends, and neat IL (without PO) was tested in a ball-on-disk tribotesting setup (Rtec instruments MFT 5000), where 50 mm diameter AISI 316L (Hardness 145 HV) disks were tested against 6.35 mm diameter alumina balls (Hardness: 400 HV), both sourced from an external vendor (McMaster Carr, USA). All disks were mechanically polished with 120, 240, 400, 600, and 1000 grit size silicon carbide polishing papers and the roughness parameter was $R_q = 0.1 \pm 0.006$ μm. The composition of the steel material and the PO, as per manufacturer, are reported in Table 1.

2.1. Synthesis of LPO

The catalytic pyrolysis of plastic was conducted using a lab-scale desk-top experimental setup (Fig. 1) as previously described by Bhoi and Rahman [6]. Initially, 20 g of ZSM-5 catalyst was loaded into the catalytic column of the double-column staged reactor. The reactor was then placed inside a split furnace, with connections made to the nitrogen gas supply and condenser. The furnace was set at the desired temperatures (A = 450 °C, B = 500 °C, and C = 550 °C, for instance). Nitrogen gas was purged at a rate of 25 mL/min to achieve and maintain the desired temperature within the reactor for one hour. Subsequently, 20 g of HDPE feedstock was introduced to the feedstock column. The condenser temperature was maintained near 0 °C by an ice-water bath. The feedstock underwent thermal decomposition in the first column, followed by the passage of volatile vapors through the second column, where ZSM-5 catalyst catalytically cracked long-chain molecules into short-chain hydrocarbons. The pyrolysis products were then condensed as pyrolysis liquids in the condenser. After approximately 30 min of experimental run time, the system was cooled to room temperature by turning off the split furnace. The yield of pyrolysis liquids was determined by collecting them in glass vials from the condenser and recording their weights. The oil constituents were analyzed using Fourier transform infrared spectroscopy (FTIR), Nuclear magnetic resonance (NMR) spectroscopy and Gas Chromatography-Flame Ionization Detection (GC-FID) techniques.

The thermochemical pyrolysis of plastics produced liquids (i.e., LPO), gaseous and solid residue. At A, B, and C temperatures, the liquid yields from plastics were 16.7 %, 30.5 %, and 20.1 %; solid residues were 3.2 %, 0.50 % and 0.00 % respectively; with a balance of gaseous yields [23]. Maximum liquid was obtained at B = 500 °C with a 96.35 % selectivity towards gasoline range hydrocarbons (C_6-C_{12}). At lower temperature (A = 450 °C), plastics were not completely decomposed producing some solid residue and lower liquid yield. At higher temperature (C = 550 °C) the liquids were further cracked to generate more gaseous yield. The detailed reaction mechanisms were previously reported by authors and could be found elsewhere [6,23]. In this research, the focus is concentrated on the obtained pyrolysis liquid's lubrication performance. These lab scale pyrolysis liquids were indicated as LPO-A, LPO-B and LPO-C that were obtained at temperatures of 450 °C, 500 °C and 550 °C, respectively.

2.2. Chemical constituents of LPO

As per the stated methodology by Rahman et al. [23] the chemical components present in the LPO was analyzed using a GC–MS system (Agilent Technologies, USA) comprising a GC (Model: 7890), inert Mass Selective Detector (MSD) with a triple-axis detector (Model: 5975), and a series injector (Model: 7683B). Qualitative analysis was performed using the Chemstation software (Agilent Technologies, USA). Identification of FID peaks was accomplished by referencing the National Institute of Standard Technology Mass Spectral (NIST MS) library [6]. To enhance the sensitivity of the MSD, a 100 μL sample of the LPO was mixed with 10 mL of dichloromethane (DCM) and the resulting diluted sample was stored in a GC–MS vial using a syringe (Catalog #0556163, Fischer Scientific, IL, USA). To remove particles larger than 0.2 μm, a 0.2 μm nylon filter (Catalog #09719C, Fischer Scientific, IL, USA) was employed. Approximately 1.5 mL of the diluted sample was required for the GC–MS analysis. For the purpose of analysis, an internal standard was prepared using 99 % vanillin (CAS #121–33–5, sourced from Alfa Aesar). A 1 % solution of vanillin was prepared in DCM by adding 100 mg of vanillin to 9900 mg of DCM, followed by a thorough mixing using an analog vortex mixer (manufactured by VWR). Finally, 15 μL of the prepared internal standard was added to the vial. For the quantification of the selectivity of the pyrolysis liquids, the Polyarc method was used [23,24]. The Concentration of the analyte was obtained using the following Eq. (1) [23,24].

$$C_A = C_S \left(\frac{Area_A}{Area_S}\right)\left(\frac{MW_A}{MW_S}\right)\left(\frac{\#C_S}{\#C_A}\right) \quad (1)$$

- where, C_A = Concentration of analyte (wt%)
- C_S = Concentration of internal standard (wt%)
- $Area_A$ = Integrated peak area of the analyte
- $Area_S$ = Integrated peak area of external standard
- MW_A = Molecular weight of analyte
- MW_S = Molecular weight of external standard
- $\#C_A$ = Carbon number of analytes
- $\#C_S$ = Carbon number of standards

The concentration of the analyte was determined utilizing the internal standard. The analyte concentration is dependent on the total sample weight, which encompasses the LPO, DCM, and internal standard. Consequently, the selectivity was computed using the following Eq. (2) [6]:

$$Selectivity\ (\%) = \frac{Concentration\ of\ compound\ detected\ (wt\%)}{Total\ concentration\ (wt\%)} \times 100 \quad (2)$$

2.3. Synthesis of IL additive

[P6,6,6,14][Sacc] was synthesized via ion exchange reaction between trihexyl tetradecyl phosphonium chloride and saccharine sodium salt hydrate [22]. The resulting product was subjected to washing steps using deionized (DI) water and dichloromethane. Separation of the water containing dissolved salt (NaCl) and the dichloromethane with the dissolved IL was achieved using a separating funnel based on density differences. Subsequently, the washed IL in dichloromethane was treated under vacuum at 80 ± 5 °C for 6 h to remove residual dichloromethane (boiling point ~40 °C) and moisture content (boiling point ~80 °C under vacuum). The dried IL was then stored at room temperature (RT) in a humidity-controlled desiccator (10 ± 5 %RH) for further use.

2.4. Characterization of PO, IL, and PO-IL blends

The characterization of each combination of PO-IL and LPO-IL was

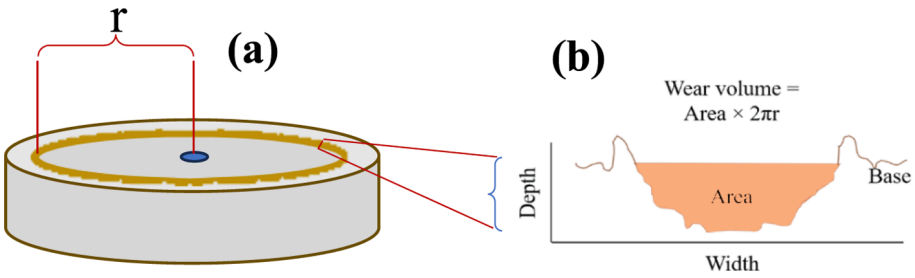

Fig. 2. (a) Schematic illustration for a worn-out metal disk, with a track radius of r, (b) 2D wear track representation to measure the wear area. Wear volume was calculated multiplying the wear area with the perimeter (2πr).

carried out using Nicolet iS^{TM} 50 FTIR. First, the background was collected using OMINIC^{TM} software before analyzing the samples. The sample was then placed on the pressure tip of FTIR under the pressure tower to collect the sample spectrum. Besides, ^{1}H NMR analyses was done for both the industrial PO and lab scale PO in a Bruker 500 MHz ^{1}H NMR, with a chloroform ($CDCl_3$) solution mixed with 0.1 % Tetramethylsilane (TMS). The results were analyzed using MestReNova software.

2.5. Property evaluation of PO, IL, and PO-IL blends

The viscosity of PO, IL and different PO-IL blends was measured using Brookfield Ametek DV2T viscometer, wherever possible, at 40 rpm, corresponding to a shear rate of 10 s^{-1}. The measured viscosity of the PO-IL blend was compared with the theoretical viscosity of the blend following modified Refutes Eq. (3) as per literature [13].

$$v_{blend} = \exp(\exp(x_{oil}.\ln(\ln(v_{oil}+0.8)) + x_{IL}.\ln(\ln(v_{IL}+0.8)))) - 0.8 \quad (3)$$

Here, v_{blend} indicates the viscosity of the blend; x_{oil}, x_{IL}, refer to the mass fraction of the oil and the IL and v_{oil}, v_{IL}, refer to the viscosity of the oil and the IL, respectively. In general, viscosity plays an important role in developing lubricating film on the surface. The thickness of the lubricating film is calculated using the Hamrock Dowson equation [13,25–27] as follows-.

$$h_0 = 3.63R'\left(\frac{U.\eta_0}{E'R'}\right)^{0.68}(\alpha E')^{0.49}\left(\frac{\omega}{E'R'^2}\right)^{-0.073}\left(1-e^{-0.68k}\right) \quad (4)$$

Here, in Eq. (4), h_0 = minimum film thickness (m); R′ = reduced radius of curvature (m); $\frac{1}{R'} = \frac{1}{R'_x} + \frac{1}{R'_y}$; η_0 = dynamic viscosity of the lubricant at the atmospheric pressure (Pa.s); U = velocity of entraining surface (m/s); $U = \frac{U_A + U_B}{2}$; U_A = velocity of ball (m/s); U_B = velocity of disk (m/s); E' = reduced young's modulus (Pa); α = pressure viscosity coefficient (m^2/N); where: $\alpha = (0.6 + 0.965\ log_{10}\eta'_0) \times 10^{-8}$; $\eta'_0 = \eta_0 \times 10^3$ *Pa.s*; ω = constant load (N); k = ellipticity parameter = 1, for point contact. A ratio between h_0 and composite root-mean-square roughness (O′*) represents the lambda (λ) ratio. $O'^* = \sqrt{(R_{q^1}{}^2 + R_{q^2}{}^2)}$, where R_{q^1}, R_{q^2} represent the root-mean-square roughness of disk ($R_{q^1} = 0.1 \pm 0.006$ μm) and the ball ($R_{q^2} = 0.05 \pm 0.006$ μm), respectively. λ ratio provides information about the lubricating regime under Stribeck curve [28,29]. λ < 1 indicates boundary lubrication where asperities rub each other extensively. For 1 < λ < 3, mixed lubrication is expected where sliding surfaces are partially separated by the lubrication film. For λ > 3, hydrodynamic lubrication is expected where the surfaces are fully separated by the lubrication film.

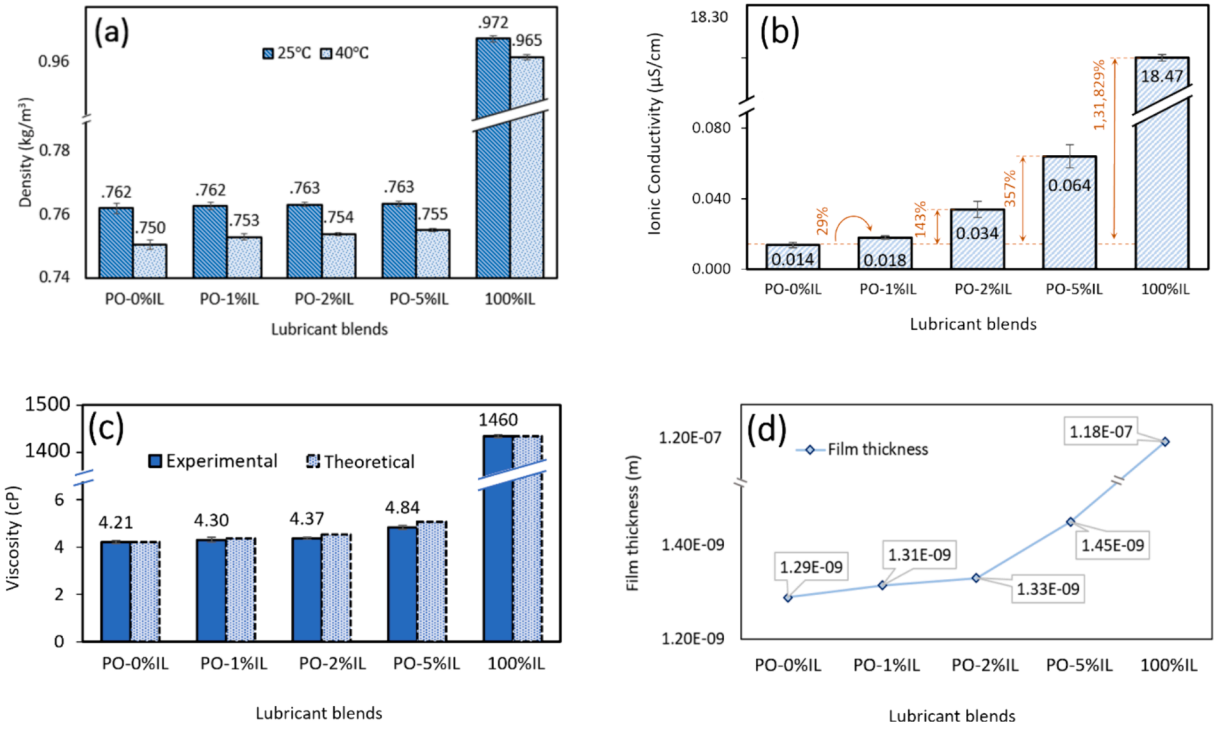

Fig. 3. (a) Density, (b) ionic conductivity, (c) experimental and theoretical viscosities, and (d) theoretical film thickness of PO, different PO-IL blends, and IL.

Wettability, ionic conductivity, and density are important physicochemical properties of ILs. These properties in base IL as well as in PO-IL blends could help better understand their lubrication mechanisms. The wettability of different lubricant samples was tested using contact angle measurement technique using Rame-Hart goniometer (Model-260, NJ, USA). A sessile droplet of 5 μl was dropped using a micro-syringe assembly on a AISI 316L sample, and the contact angles were detected by a 750 FPS superspeed U2 series upgrade kit (p/n 100-12-U2), all manufactured by Rame-hart, NJ, USA. Further, the ionic conductivity of the PO-IL blends was measured using a Metler Toledo seven compact duo conductivity meter and a platinum electrode. The density was measured using a Metler Toledo weighing device using Archimedes principle [30].

2.6. Tribological tests

The friction and wear performance of different lubricant blends were tested in a multifunctional tribometer (Rtec, CA, USA) under ball on disk setup, following the procedures of ASTM G-99 standard, for 0.1 m/s speed, 40 N load, 2.7 GPa Hertzian contact pressure, 1 h duration and 1 km linear distance. These parameters were selected to match and compare the results of the prior experiments done by the authors [12,28]. Similar parameters are employed in typical applications of hybrid bearings and wind turbine gearbox where lowering the friction and wear is essential [22,31,32]. For reproducibility, each test was repeated at least twice. The stable friction values of last 20 min were used for comparison. The wear volume was calculated from the 2D optical image, obtained from a confocal profilometer (attached to the multifunctional tribometer) using the formula shown in Fig. 2.

The specific wear rate of the steel samples was determined by calculating the wear volume and dividing that with 'load times sliding distance', as shown in Eq. (5). To begin, the area of the wear profiles was obtained through integration. In this process, the base line was utilized to determine the actual worn area by excluding the wear debris, as illustrated in Fig. 2 [30]. Subsequently, the calculated area of the wear profile was multiplied by the length (2πr) of the wear track to obtain the wear volume [30]. This procedure was repeated a minimum of three times on a wear track to compute the average wear rate.

$$specific\ \ wear\ \ rate = \frac{Wear\ \ volume}{Load \times Sliding\ \ distance} \tag{5}$$

3. Results

The physicochemical and tribological properties of PO-IL, and LPO-IL blends were tested using the experimental methodologies described above and their experimental results are presented in the following subsections.

3.1. Physicochemical property evaluation of PO, IL and PO-IL blends

Density of five lubricants (PO, PO-1 %IL, PO-2 %IL, PO-5 %IL, IL) were tested at room temperature (25 °C) as well as at 40 °C and the results are presented in Fig. 3(a). It was observed that for base PO, the density was much lower than neat IL. For example, at room temperature, the density of PO was 0.762 kg/m^3 whereas for IL it was 0.972 kg/m^3. This value is similar to that observed in earlier literature [30]. As the concentration of IL increased in the blend, the density slightly increased. Also, for each case, the density reduced at 40 °C for all PO-IL blends. It shows that the density of tested PO-IL blends (PO-1–5 %IL) was much lower than neat IL, meaning there will be less mass of PO-IL blend required for a lubrication application to cover same volume compared to neat IL.

Ionic conductivity is an important property of oils, especially for ILs. Neat ILs are made up with anion and cations and as the ions move within the bulk, they transfer charge that makes ILs conductive. Such conductivity in a dilute solution can impose interesting aspects such as

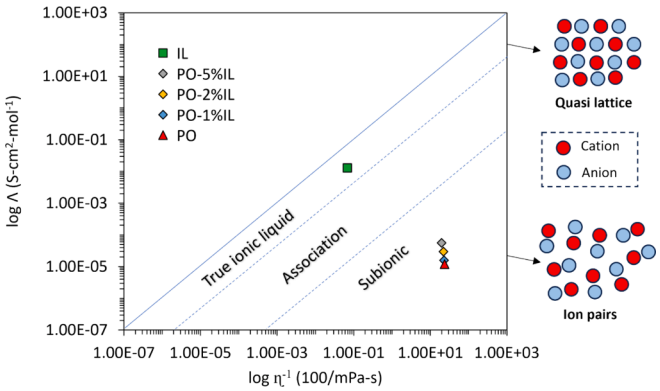

Fig. 4. Walden plot for PO, IL, and different PO-IL blends, where the vertical axis represents the logarithmic molar conductivity (Λ) and the horizontal axis represents the inverse of viscosity in logarithmic scale.

dissociation and ionicity. The ionic conductivity results of PO, IL and PO-IL blends are presented in Fig. 3(b). It is seen that the neat IL possess a conductivity of 18.47 μS/cm, which is 1,31,829 % higher than the base PO (0.014 μS/cm). When IL mixed with PO, the conductivity of PO-IL blends was increased significantly.

The viscosity of the five PO-IL blends was measured at room temperature and presented in Fig. 3(c). It was observed that the viscosity of PO is much lower (4.21 cP) compared to IL (1460 cP). Similar values were previously reported for PO and IL, in the literature [12,30]. Viscosity of PO-IL blends was slightly increased by adding different percentage of IL and their values showed similar results as calculated theoretically using Refutas Eq. (3), as shown in Fig. 3(c). The film thickness associated with each PO, IL and PO-IL blend is calculated using Eq. (4) and presented in Fig. 3(d). It was observed that for the base PO sample, the film thickness was 1.28 nm whereas for neat IL, it was 118 nm. The film thickness increased from 1.31 nm to 1.45 nm as the percentage of IL additive was varied from 1 to 5 % in the base PO.

In general, for ionic solutions, viscosity has an inverse relationship with associated ionic conductivity [13]. For instance, a higher viscosity restricts the mobility of ions and therefore the ionic conductivity reduces. In the PO-IL blends, a subtle change (1–5 %) in IL percentage actually increased the conductivity of PO by 29–357 %, respectively. Interestingly, when the viscosity of the blends increased (Fig. 3c), the ionic conductivity (Fig. 3b) followed the same trend.

The change of conductivity for a change of viscosity is an important phenomenon that can be represented using a Walden plot as shown in Fig. 4. Walden plot is used in electrochemical systems to understand the association tendency of ions in a solution. If the viscosity of a solution decreases linearly with its ionic conductivity, the graph matches the diagonal line [33]. An ionic solution is considered to be true in nature (the ions are unassociated and oriented in a quasi-lattice) if its location is close to the diagonal. If the solution is located well below the diagonal, it is often termed as subionic, where the ions are paired with the opposite ions (anion-cation pairs). For these solutions, the conductivity and viscosity not necessarily vary linearly. In Fig. 4, the Walden plot for PO, IL and PO-IL blends are presented where the vertical axis represents the molar conductivity ($\Lambda = \sigma M/\rho$) and the horizontal axis represents the inverse of viscosity. Here, σ = ionic conductivity, M = Molecular weight of IL, ρ = Density of the solution (PO, IL and PO-IL blends). It is observed in Fig. 4 that the IL offers a true nature, meaning the ions are oriented in quasi lattice [33]. On the other hand, all the PO-IL blends are positioned in the sub-ionic zone. The change of IL concentration from 0 to 1 % slightly increased the molar conductivity (the red and blue dots are very adjacent), however for 2 % and 5 % concentration, the change of molar conductivity was significant with respect to the slight increase in viscosity (The yellow and ash dots are far from the blue one). Such change could be linked to ion dissociation tendency in PO-IL blends, which

Fig. 5. Contact angle representation of PO and IL on steel surface after one minute duration.

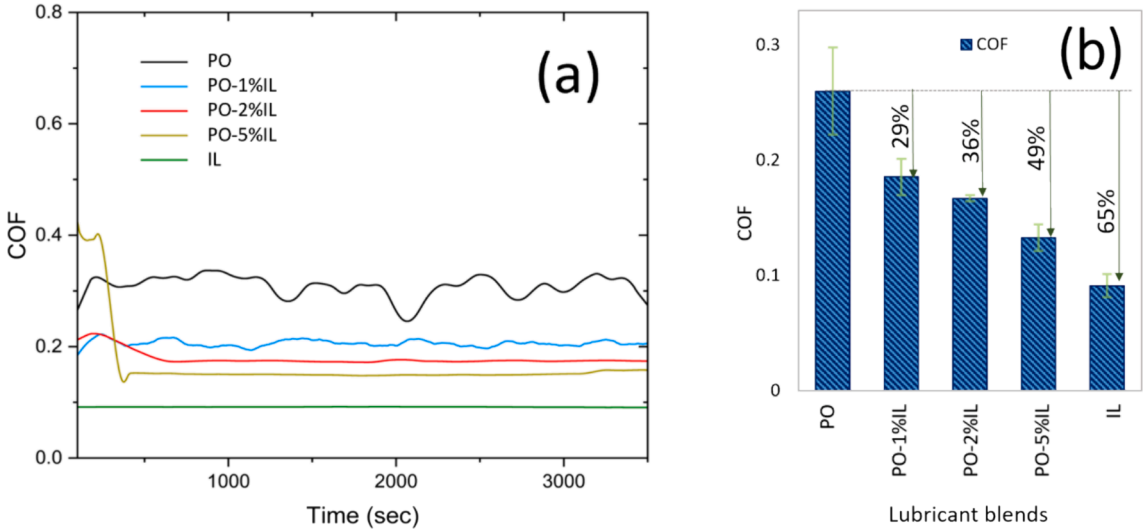

Fig. 6. (a) Variation of COF with time for PO, IL and different PO-IL blends over one hour, (b) average COF of PO, IL and different PO-IL blends.

increased the ionicity with higher IL concentration [34]. Ionic dissociation is often linked with the formation of solvation cell and micelle which has great impact on lubrication process [35]. The role of ion dissociation in the lubrication mechanism is discussed in the later part of this paper.

Fig. 5 shows a contact angle representation for PO and IL at room temperature after one minute. It was observed that PO spread on the steel surface very fast and the contact angle reaches below 5 degrees within few seconds. After about one minute, the contact angle went below 2° and could not be detected anymore. The contact angle reflects the balance between adhesion and cohesion interaction forces. Adhesion is the attraction between liquid and the surface, whereas cohesion is the attraction within the liquid molecules. Higher adhesion than cohesion typically provides fast spreading ability and lower contact angle of oil on metallic surface [22]. On the other hand, higher cohesion than adhesion increases the contact angle [13]. Compared to PO, the IL experienced a higher contact angle (~40° after 5 s and ~15° after 60 s). This indicates that the PO has higher adhesion interaction energy than IL, whereas IL has higher cohesion energy than PO.

3.2. *Tribological performance of PO-IL blends*

The tribological performance of different PO-IL blends were tested at room temperature using a pin on disk setup. Fig. 6(a) represents the variation of coefficient of friction (COF) with time for various PO-IL blends and Fig. 6(b) shows the average COF. It is observed in Fig. 6(a) that the fluctuations in COF minimized by adding IL additive. Fig. 6(b) shows that PO, and IL provided COF of 0.26 and 0.09, respectively. With an addition of 1 %, 2 % and 5 % IL into PO, the COF was reduced by 29 %, 36 % and 49 %, respectively, compared to base PO. The λ ratio for PO, PO-1 %IL, PO-2 %IL and PO-5 % IL were less than 1, indicating that the tests are conducted under boundary lubrication regime. On the other hand, for IL, the λ ratio was between 1 and 3, indicating that the tests are under mixed lubrication regime.

The wear tracks of PO, IL and different PO-IL blends are presented in Fig. 7. The specific wear rate was calculated from these images using Eq. (5). As shown in Fig. 7(a) the PO was unable to protect the surface and therefore the wear track was wide. There were abrasive marks present due to plowing action by the harder ball. Also, there were prominent ridge formation observed. The width of the wear track significantly reduced with the addition of 1 %, 2 %, and 5 % IL (Fig. 7(b–d)). For neat IL (Fig. 7(e)) the wear track was very narrow. Fig. 7(f) represents the wear rates of PO, IL and different PO-IL blends. The wear rate of PO was 1.61×10^{-4} mm^3/N.m and by adding 1 %, 2 %, and 5 % IL, the specific wear rate was reduced by 36 %, 76 % and 81 % respectively. Neat IL provided a specific wear rate of 2.51×10^{-6} m^3/N.m, which was 99 % less than base PO.

The base PO exhibited significant wear which could be attributed to their low viscosity. As a result, the lubrication film was not able to separate the asperity-asperity contact and therefore the real area of contact was significant, leading to severe wear, as shown in the SEM image in Fig. 8(a). Compared to PO, PO-2 %IL wear track was less wide, as seen in Fig. 8(b). Neat IL provided a very shallow wear track (Fig. 8 (c)) due to the thick lubricating film formed at the tribological interface [22].

The comparative improvement scenario for COF and specific wear rate of PO, IL and different PO-IL blends is provided in Table 2. Here, although a gradual reduction in COF and specific wear rate was noticed with increased IL concentrations, it is clear that the incorporation of 2 % and 5 % IL gave significant reduction in COF and specific wear rate than base PO. It was observed that 2 % IL improved the COF by 36 % and the wear rate by 76 % compared to base PO. On the other hand, adding another 3 % IL (PO-5 %IL) improved the COF by another 20 % and the specific wear rate by another 20 % only. Considering the cost associated with 5 % IL (which is 2.5 times more than 2 % IL), the benefit is insignificant. Therefore 2 % IL concentration was considered for further tribological experimentations with LPO samples.

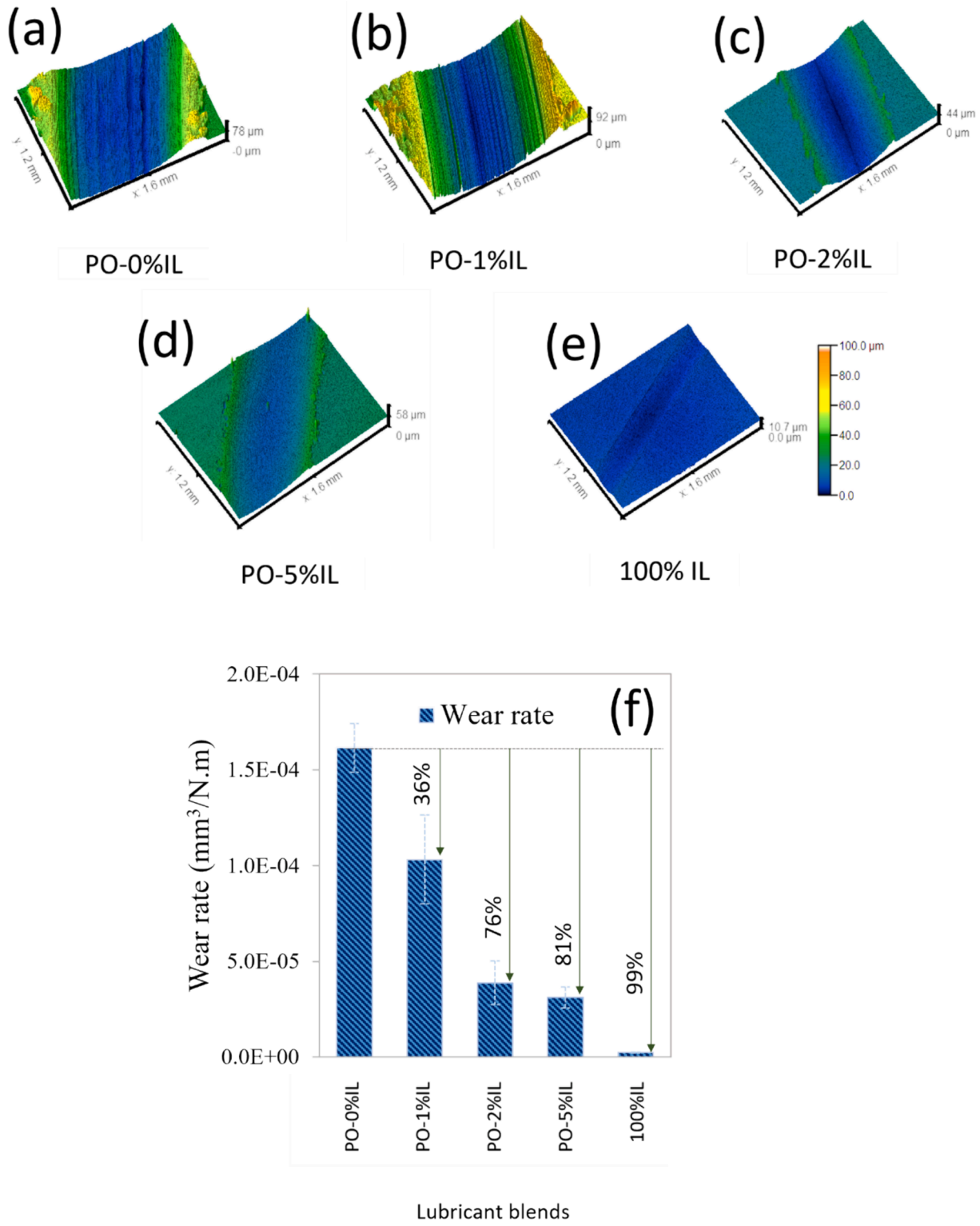

Fig. 7. Three-dimensional wear profiles for (a) PO (b) PO-1 %IL, (c) PO-2 %IL, (d) PO-5 %IL, and (e) IL; (f) specific wear rates for PO, IL and different PO-IL blends.

3.3. Tribology of different plastic derived oils and blends

Fig. 9 represents the comparison between different types of plastic derived oil's (a) COF variation with time, and (b) average COF. These plastic derived oils include industrial PO and LPO, without the IL additives. As shown in Fig. 9(a), the industrial PO experienced significant fluctuations (black line), whereas for all the LPO samples, the fluctuations were subtle. As shown in Fig. 9(b), all the LPO samples provided significantly less COF (36–56 %) than the PO, whereas the COF associated with LPO-C was lowest.

Fig. 10(a–c) represents the three-dimensional wear track profiles for different LPO samples. LPO-A shows less wide wear track than LPO-B and LPO-C. All the wear tracks generated with LPO lubricants were shallower than the PO lubricants as shown in Fig. 7(d). Fig. 10(e) shows the specific wear rate calculated from Fig. 10(a–d) of different lubricant samples and compares their difference with respect to PO. It is observed

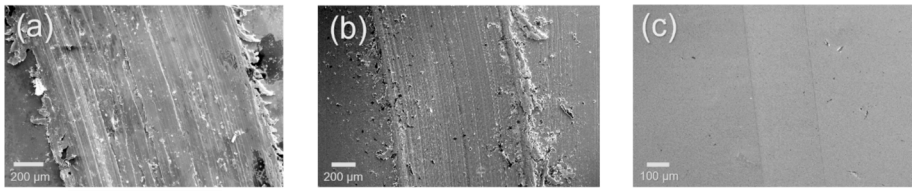

Fig. 8. SEM images of wear tracks from (a) PO, (b) PO-2 %IL, and (c) IL.

Table 2
COF and wear results for different PO-IL blends.

	COF	% Change	% Change in consecutive steps	Specific wear rate ($mm^3/N.m$)	% Change	% Change in consecutive steps
PO	0.26	0	0	1.61×10^{-4}	0	0
PO-1 %IL	0.19	28.6	28.6	1.03×10^{-4}	36.1	36.1
PO-2 %IL	0.17	35.8	10.0	3.88×10^{-4}	76.0	62.4
PO-5 %IL	0.13	48.9	20.4	3.12×10^{-5}	80.7	19.6
IL	0.09	64.9	31.3	2.51×10^{-6}	98.5	92.0

in Fig. 10(d) that the LPO-A experienced 89 % lower wear rate than PO whereas LPO-B and LPO-C experienced 72 % and 75 % lower wear rate respectively than base PO.

Fig. 11(a) shows how the COF varies with time for different lubricant blends with 2 % IL, and Fig. 11(b) shows the average COF of different base oils derived from plastics, and their blends with 2 % IL. It is seen in the Fig. 11(a) that the incorporation of 2 % IL in base LPO exhibits significantly less COF than incorporating 2 % IL in base PO (black line). The quantitative improvements (% change in COF due to the IL addition) are shown in Fig. 11(b) and tabulated in Table 3. It was observed that 2 % IL addition to PO, LPO-A, LPO-B, LPO-C samples improved the COF performance by 36 %, 26 %, 17 %, and 50 %.

Fig. 12(a–c) shows the optical profilometer images of the wear tracks from different LPO-2 %IL blends. After 2 % IL addition, the wear tracks got shallower, and the ridge formation was less prominent for all LPO-2 %IL blends compared to PO-2 %IL blend shown in Fig. 12(d). The specific wear rate of different base oils derived from plastics without and with 2 % IL blends are compared in Fig. 12(e) and tabulated in Table 3. It can be observed in Fig. 12(e) that the PO-2 %IL, LPO-A-2 %IL, LPO-B-2 %IL, LPO-C-2 %IL experienced 76 %, 28 %, 73 %, and 75 % less wear rate than PO, LPO-A, LPO-B, LPO-C respectively.

Table 3 represents the % difference in COF and wear rate for different lubricant blends before and after adding 2 % IL. Interestingly, among other LPO-IL blends, the lowest COF and wear were observed for LPO-C-2 %IL, which provided 50 % lower COF and 75 % lower wear rate than base LPO-C.

To understand the wear mechanism, the SEM micrographs for LPO-C, and LPO-C-2 %IL samples are compared in Fig. 13(a–b). It is observed for LPO-C (Fig. 13(a)) that the abrasive marks were present inside wear tracks indicating the abrasion mechanism of wear due to the hard ball scratching the softer disk surface. The incorporation of IL in the plastic derived base oils, reduced the abrasive marks. Besides, In Fig. 13(a), surface delamination was observed which was not seen in presence of the IL additive in Fig. 13(b). Therefore, IL additive was successful in reducing the wear rate significantly overall.

Table 4 represents the EDX analysis of different lubricant blends of plastic derived oil and IL. As it was expected, the samples for 2 % IL offered higher proportion of P and S which indicates the presence of a P

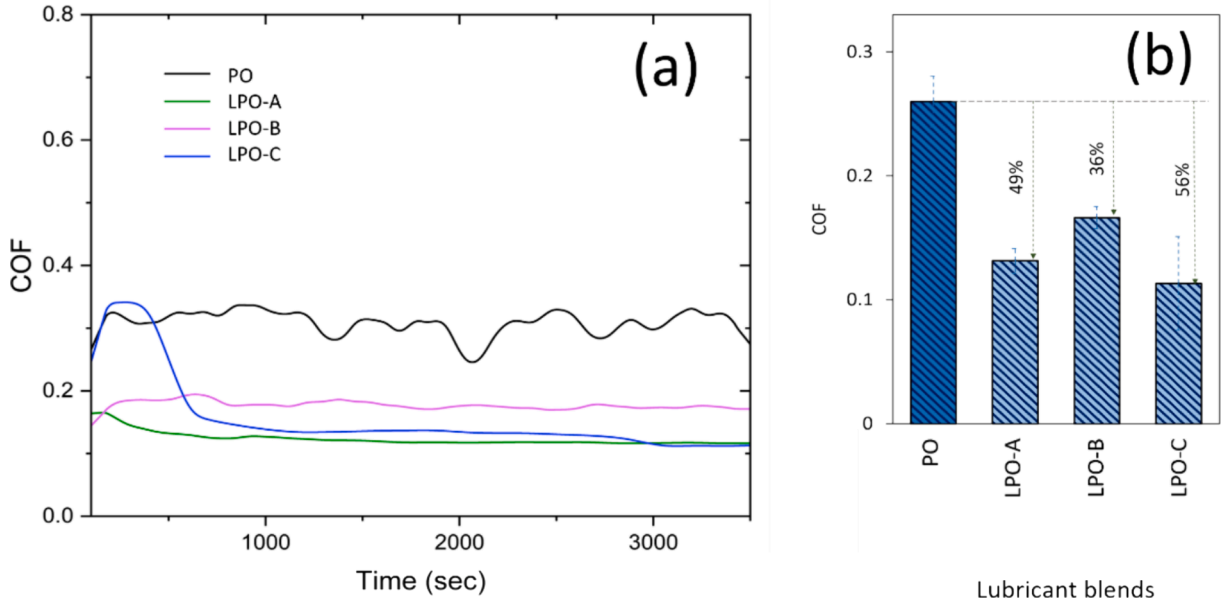

Fig. 9. (a) Variation of COF with time, and (b) average COF of different types of base oils derived from plastics.

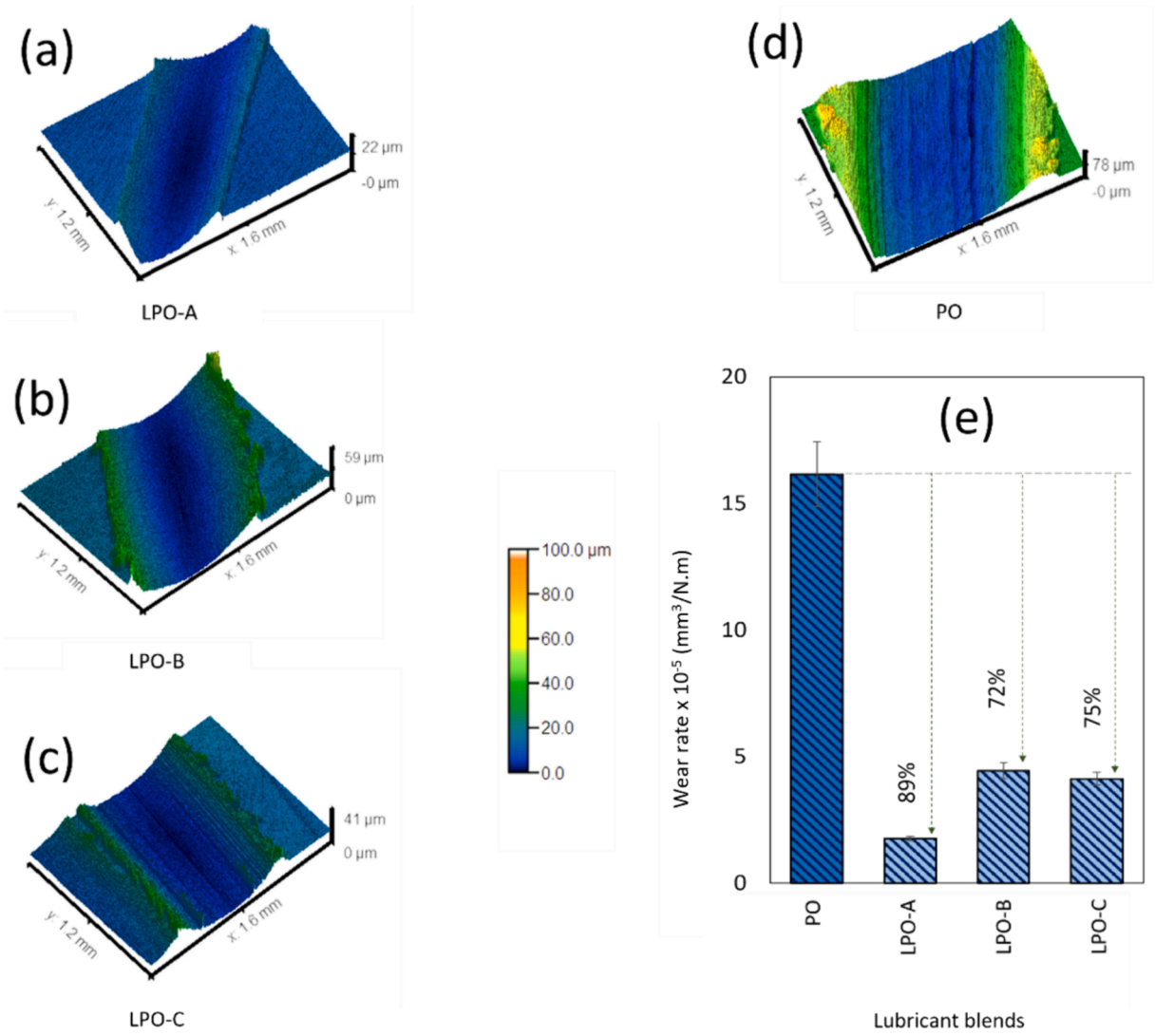

Fig. 10. Three-dimensional wear profiles of worn surface with (a) LPO-A (b) LPO-B, (c) LPO-C, (d) PO; (e) specific wear rates for different types of base oils derived from plastics.

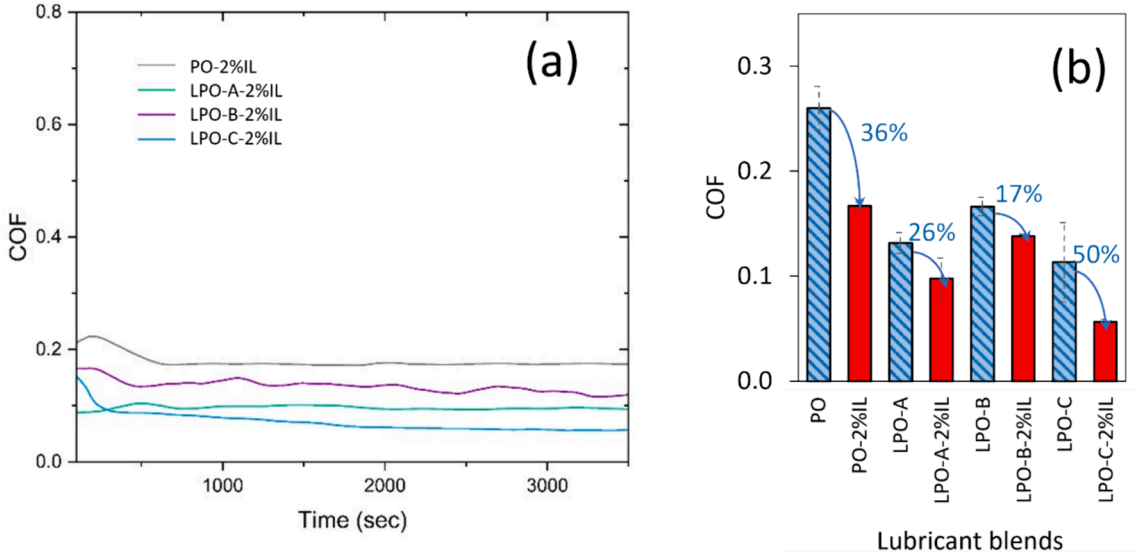

Fig. 11. (a) Variation of COF with time, and (b) average COF of different types of base lubricants without any IL and with 2 % IL.

Table 3
COF and wear comparison for different lubricant blends of plastic derived oils and IL.

	COF	%change	Sp. wear rate (mm^3/N.m)	%change
PO	0.26	35.8	1.61×10^{-4}	76
PO-2 %IL	0.17		3.88×10^{-5}	
LPO-A	0.13	25.8	1.76×10^{-5}	
LPO-A-2 %IL	0.10		1.27×10^{-5}	28.1
LPO-B	0.17		4.44×10^{-5}	
LPO-B-2 %IL	0.14	16.9	1.20×10^{-5}	73.1
LPO-C	0.11	50.2	4.12×10^{-5}	74.6
LPO-C-2 %IL	0.06		1.05×10^{-5}	

and S rich tribofilm that was able to reduce the friction and wear [36]. Besides, the presence of O in overall worn samples indicated the formation of oxides (iron oxide, phosphorous oxide, etc).

3.4. Chemical characterization of different lubricant blends

Lubrication mechanisms of different lubricant blends depend on the presence of chemical groups in the blend. FTIR analyses were performed to identify the functional groups present in PO, IL, different PO-IL, and different LPO-IL blends. The functional groups present in different lubricants and their blends are presented in Table 5. As observed in Table 5, all the oil samples derived from plastics possess alkyl sp^3 bonds whereas the aromatic ring peaks between 1450 and 1650 cm^{-1} were not observed in the industrial PO sample, and were only present in the LPO samples [12,23]. As a result, the PO was solely a mixture of saturated hydrocarbons, whereas the LPO samples contained unsaturated hydrocarbons.

Miscibility is an important aspect of lubricant blends, that refers to the ability of different substances to mix completely to form a solution. It is worth noting that the IL was partially miscible in the industrial PO, and completely miscible in LPO samples. This is because the presence of double bonds in unsaturated hydrocarbons allowed for more efficient packing of molecules in the liquid state, making them more likely to mix with unsaturated IL molecules in LPO. The saturated solution of PO was able to partially mix the unsaturated aromatic rings of IL, therefore created two separate layers after four weeks of mixing. Each layer was separately characterized by FTIR, and the presence of the aromatic ring was confirmed for both the top (solution) and bottom layers (precipitate) as reported in Table 5. For lubrication, it is not unusual for IL additives in base oil to create separate layers because of limited miscibility

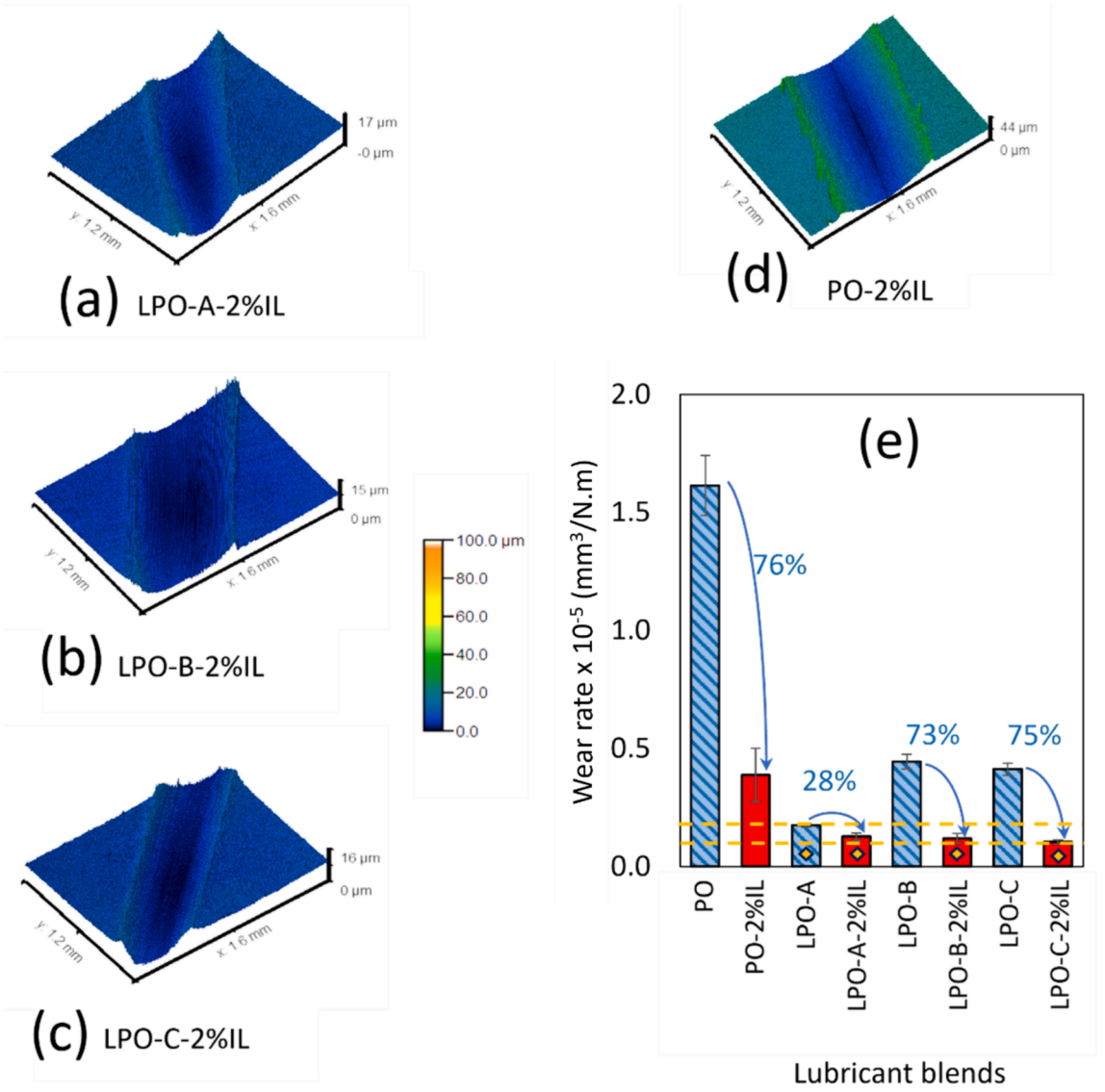

Fig. 12. Three-dimensional wear profiles of worn surface with (a) LPO-A-2 %IL, (b) LPO-B-2 %IL (c) LPO-C-2 %IL, (d) PO-2 %IL, (e) specific wear rates for different base lubricant without any IL and with 2 % IL.

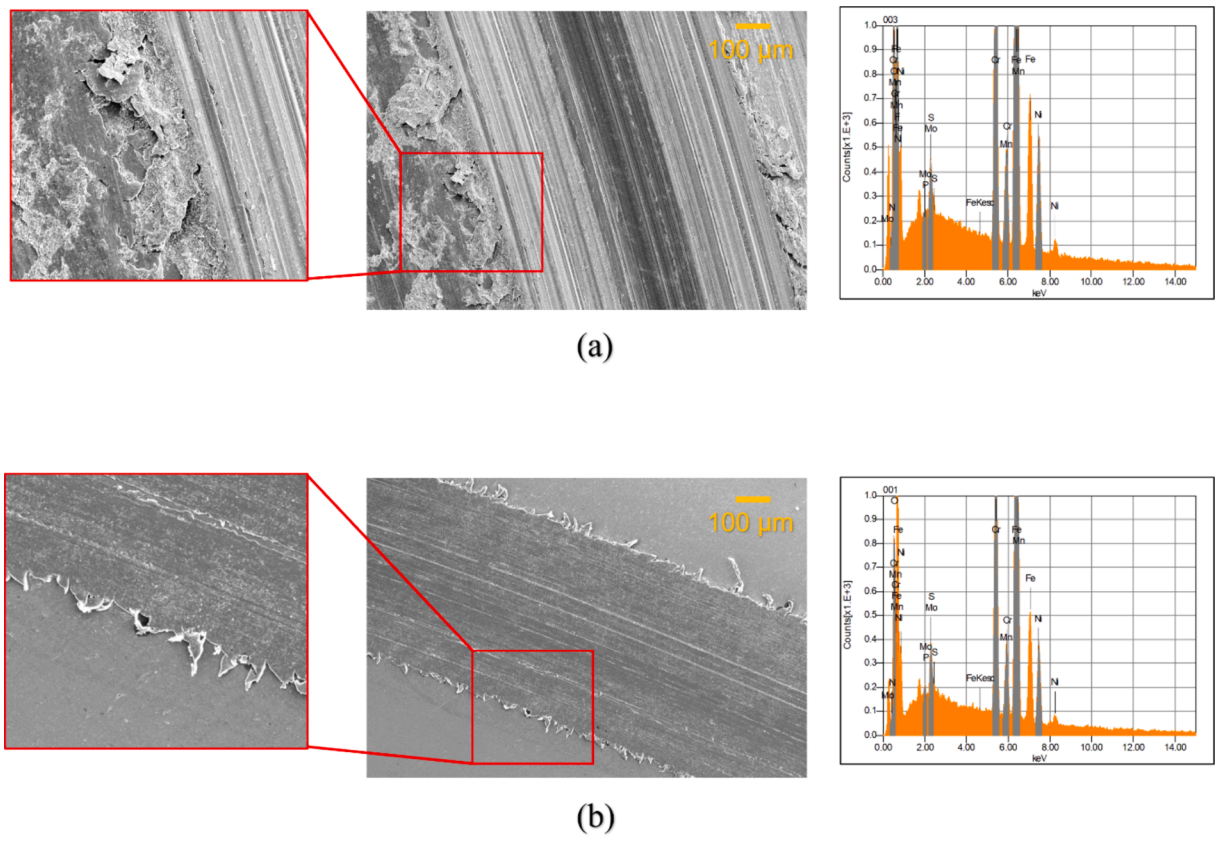

Fig. 13. SEM micrographs and EDX elemental maps for (a) LPO-C and (b) LPO-C-2 %IL.

Table 4
EDX analysis on the wear track of the steel samples tested with different base oils derived from plastics and their blend with 2% IL additives.

	PO	PO-2 %IL	LPO-A	LPO-A-2 %IL	LPO-B	LPO-B-2 %IL	LPO-C	LPO-C-2 %IL
	Mass%							
N	0.78	0.08	0.87	0.83	1.00	0.52	0.84	1.18
O	2.33	0.18	1.90	9.77	4.63	3.39	3.16	3.76
P	0.06	0.43	–	0.09	0.07	0.14	0.09	0.19
S	–	0.57	0.11	0.94	0.07	0.94	–	0.22
Cr	17.13	18.37	18.15	17.22	17.01	17.64	17.17	17.57
Mn	1.87	1.28	1.09	–	1.89	1.09	1.40	1.89
Fe	65.63	68.84	66.19	60.84	63.50	66.43	64.49	63.38
Ni	9.44	9.67	9.99	9.40	9.74	9.29	9.63	9.38
Mo	2.74	0.57	1.70	0.91	2.10	0.56	2.23	2.42

[37]. While tribo-testing, due to the interaction between the tribo-pair, both layers get mixed together and the additives in the bulk fluid can improve the overall lubrication performance.

The absence of the aromatic ring in the PO was further confirmed by ^{1}H NMR. As shown in Fig. 14(a), there was no peak between the 6 and 8 ppm region (except reference-$CDCl_3$). On the other hand, Fig. 14(b) contains peaks between the 6 and 8 ppm region, confirming the presence of aromatic compounds. All these characterizations show a clear difference between the industrial PO and LPO in terms of the aromatic compound's presence.

3.5. Chemical constituents of LPO

The chemical constituents of the LPO-A, LPO-B, and LPO-C samples were further investigated in the GC-FID. Table 6 depicts their chemical compositions. It was observed that higher temperature had higher selectivity towards aromatic hydrocarbons with a lower carbon number (#C). This observation is due to higher temperature promoted more thermal cracking than lower temperatures [23]. For instance, methylbenzene (C_9) and indene (C_{10}) were the main constituents in LPO-A whereas for LPO-B, the constituents were mostly methylbenzenes (C_9), which are similar to that of commercial gasoline [23]. Also, in LPO-B, a slight proportion of alkene (1-Nonadecene) was identified. In LPO-C, varieties of alkylbenzenes (C_7- C_9) were obtained including toluene (C_7), and xylene (C_8). Additionally, a slight proportion of acrylamide (2-propenamide) was detected.

Overall, all the LPO lubricants contain aromatic ring structures. The selectivity percentage of aromatics for three LPO lubricants were: LPO-A (100 %) > LPO-C (99.10 %) > LPO-B (96.35 %). In contrast, the industrial PO sample didn't contain any aromatic structure in its formulation. This contrast indicates the influence of aromatic structures regarding the lubrication performance of LPO. The discussion on tribological results and the lubrication mechanism of different blends are provided in the following sections.

4. Discussion

The analysis in the preceding section showed that tribological

Table 5
FTIR analysis of the lubricant blends (PO, PO-1 % IL, PO-2 % IL, PO-3 % IL, PO-5 %IL, IL, LPO-A, LPO-A-2 % IL, LPO-B, LPO-B-2 % IL, LPO-C, and LPO-C-2 % IL).

Chemical compounds	Frequency Range (cm^{-1})	Functional group	Mixed condition	PO	PO-1 % IL	PO-2 % IL	PO-5 % IL	IL	LPO-A	LPO-A-2 %IL	LPO-B	LPO-B-2 %IL	LPO	LPO-C-2 %IL
Zone 1	**3700–3200**													
Alcohol	3650–3200	—O—H	Solution	x	x	x	x	x	x	x	x	x	x	x
			Precipitate	x	x	x	x	x	*	*	*	*	*	*
Zone 2	**3200–2690**													
Aryl or vinyl sp2 C—H bond	3100–3000	≡C—H	Solution	x	x	x	x	x	✓	✓	✓	✓	✓	✓
			Precipitate	x	x	x	x	x	*	*	*	*	*	*
Alkyl sp3 C—H bond	2960–2850	≡C—H	Solution	✓	✓	✓	✓	✓	✓	✓	✓	✓	✓	✓
			Precipitate	✓	✓	✓	✓	✓	*	*	*	*	*	*
Carboxylic acid	3000–2500	—COOH	Solution	x	x	x	x	x	x	x	x	x	x	x
			Precipitate	x	x	x	x	x	*	*	*	*	*	*
Zone 3	**2380–1990**													
Alkyne	2260–2000	–C≡C—	Solution	x	x	x	x	x	x	x	x	x	x	x
			Precipitate	x	x	x	x	x	*	*	*	*	*	*
Zone 4	**1850–1700**													
Ketone	1750–1705	=C=O	Solution	x	x	x	x	x	x	x	x	x	x	x
			Precipitate	x	x	x	x	x	*	*	*	*	*	*
Aldehyde	1740–1720	>C=O	Solution	x	x	x	x	x	x	x	x	x	x	x
			Precipitate	x	x	x	x	x	*	*	*	*	*	*
Zone 5	**1650–1450**													
Alkene	1650–1620	=C=C=	Solution	x	x	x	x	x	x	x	x	x	x	x
			Precipitate	x	x	x	x	x	*	*	*	*	*	*
Benzene	~1600 and ~1500		Solution	x	✓	✓	✓	✓	✓	✓	✓	✓	✓	✓
			Precipitate	x	✓	✓	✓	✓	*	*	*	*	*	*
C—H bend stretching vibration presence of alkenes	1470–1450	≡C—H	solution	✓	✓	✓	✓	✓	x	x	✓	✓	✓	✓
			Precipitate	✓	✓	✓	✓	✓	*	*	*	*	*	*

* Precipitate layer was not obtained.

properties improved as a result of three factors: (i) physicochemical properties of IL additive, namely: viscosity, density, ionic conductivity (ii) molecular structures present in different plastic derived oils, and (iii) interfacial property, such as wettability, and tribofilm formation. The effects of these factors are discussed in the following sub-sections.

4.1. Influence of physicochemical properties of additive on the tribological performance

The physicochemical properties of IL additive played an important role to enhance the tribological performance of plastic derived oil. Especially, the addition of IL increased the viscosity of the lubricant blends and that in return provided thicker film, thereby reducing asperity-asperity contact. As a result, the friction and wear both were significantly reduced. Ionic conductivity has also played a significant role to enhance the tribological performance of the studied lubricant blends. The increase in conductivity for an increase in viscosity showed dissociation tendency of IL ions [35]. These ions in presence of moisture, agglomerated with the constituents of plastic derived oil and formed ionic shell. It was previously reported that the dried [P6,6,6,14][Sacc] can contain 425 ppm moisture [38]. Also, pyrolysis process of oil extraction accumulates water while oil condensation takes place [7]. The trihexyl tetradecyl phosphonium cation of IL is hydrophobic whereas, saccharinate is slightly hydrophilic [39]. Such a mix of hydrophobic head and hydrophilic tail often helps in micelle formation through entangling with water molecules present in the lubricant [39,40]. Moreover, the IL used in this study was bio-based, which complies nicely with the sustainability perspective of utilizing plastic derived oils. Therefore, this study shows that by incorporating [P6,6,6,14][Sacc] IL additive, plastic derived oils could be utilized for next generation lubrication in automotives and other industries.

4.2. Influence of chemical structures on tribological performance

The chemical structures present in the plastic derived oil play a major role to determine the overall tribological performance. Aromatic structures contain carbons in the ring, that help the associated chemical species to adsorb to the steel surface due to the C-Fe interaction [22]. As a result, the aromatic structures of all base LPO were overall more favorable to reduce friction and wear between tribo-pair than aliphatic chemical structures, present in the PO lubricant. For this same reason, IL additive, which contains an aromatic double ring structure, reduced the friction and wear rate significantly in PO-IL and LPO-IL blends.

It is interesting to see that for LPO-A, the incorporation of 2 % IL reduced the wear rate by only 28 %, whereas for LPO-B and LPO-C, the incorporation of 2 % IL reduced the wear rate by 73 %, and 75 % respectively (Fig. 12). The reason of such contrast between LPO-A with other LPO-IL blends could be explained if the wear rate of LPO-A is taken into consideration. The LPO-A sample's wear rate was already less than PO by 89 % (Fig. 10(e)). In compared to that, the LPO-B and LPO-C exhibited 72 and 75 % less wear rate than PO (Fig. 10(e)). The overall improvement of all base LPO over base PO was attributed to the presence of aromatic ring structure in LPO and the absence of such structures in the PO, as discussed earlier. Specifically, if the chemical structures present in LPO-A is considered, then the reason behind the lowest wear rate for LPO-A than all other base oils can be explained. While looking into the chemical constituents of the LPO-A, the presence of 2,3-dihydro-5-methyl-1H-Indene (double ring indene ) was observed, which possess a double aromatic ring structure, similar to the saccharinate portion of the IL additive. That double ring aromatic structure significantly reduced the friction and wear rate of LPO-A among all LPO samples. This finding supports the positive influence of double ring

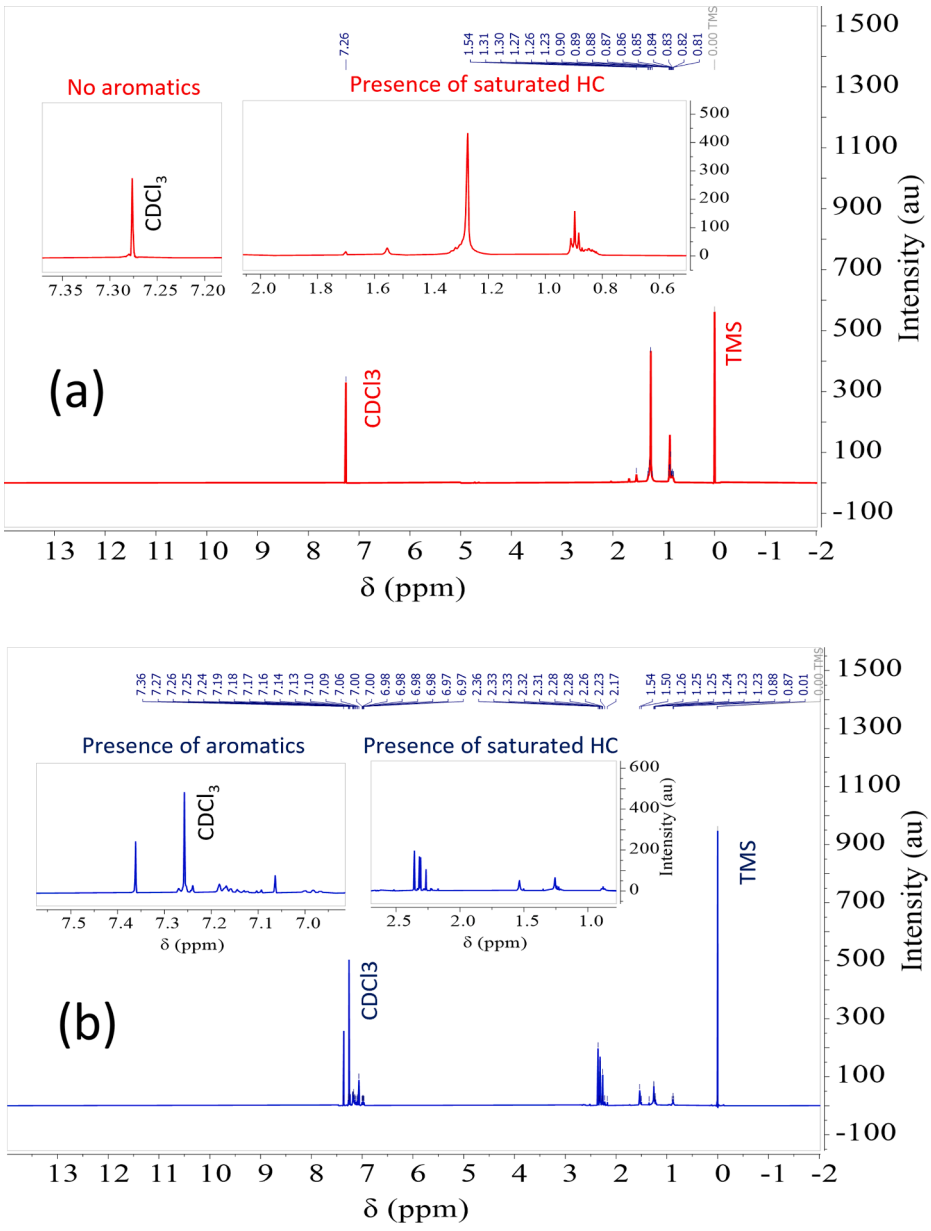

Fig. 14. ^{1}H NMR for (a) industrial PO and (b) lab synthesized PO (LPO-A).

structured molecules in improving the wear performance of plastic derived oils. As a result, in Fig. 12(e), the wear rate of LPO-A was similar to those of LPO-2 %IL blends (yellow dotted lines in Fig. 12(e)). Further, LPO-A-2 %IL offered 28 % lower wear rate than LPO-A. This could be attributed to the synergistic effect between LPO and IL additives. Previously, it was reported that the tribological performance gets improved for lubricants with a mixture of aromatic along with aliphatic, compared to aromatic or aliphatic alone [22,41]. The IL containing aliphatic long alkyl group incorporated the necessary straight chain constituents in the lubricant blends. Besides, the long alkyl chains contain carbons in the sp^3 C—H bonds that help the IL moieties to adsorb to the steel surface due to the C-Fe interaction [22]. As such, the wear was reduced for LPO-A-2 %IL than LPO by 28 %. A similar analogy explains the reason behind the best performance of LPO-C-2 %IL among all LPO-2 %IL blends. The LPO-C already contained 99.1 % aromatics (Table 6), along with 0.9 % aliphatic (2-propenimide). The incorporation of 2 %IL with double aromatic ring reduced the wear rate to achieve the best performance. Overall, the single and double aromatic rings, along with straight aliphatic chains were favorable to reduce the friction and wear rate to the lowest for LPO-C-2 %IL among all lubricant blends.

4.3. *Influence of the interfacial properties on the tribological performance*

The wettability behavior of plastic derived oil and IL additive showed that the IL possesses higher contact angle, and therefore higher cohesion interaction energy than plastic derived oils. As a result, the incorporation of IL to the plastic derived oils enhanced the cohesion interaction energy of the blend [22]. PO, on the other hand possess lower contact angle than IL, and therefore demonstrate stronger adhesion interaction with the surface. As a result, the PO-IL lubricant blends provided conjugal action of strong adhesion and strong cohesion. These actions helped in strong adsorption film formation on steel surface, which improved the tribological performances of lubricant blends compared to base oils [22].

Moreover, interfacial tribofilm played a role on the tribological performance. The presence of P, S content in the wear track with 2 % IL samples (Table 4) showed that while tribological interaction took place, a chemically reactive tribofilm was generated which could be attributed

Table 6
Composition of LPO-A, LPO-B, and LPO-C with selectivity percentages.

Identified compound	Structure	Chemical formula	LPO-A 450 °C	LPO-B 500 °C	LPO-C 550 °C
2-Propenamide	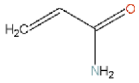	C_3H_5NO	–	–	0.90 %
Toluene		C_7H_8	–	–	44.72 %
p-Xylene		C_8H_{10}	–	–	32.61 %
Benzene, 1-ethyl-2-methyl-		C_9H_{12}	–	45.13 %	11.37 %
Benzene, 1,2,3-trimethyl-		C_9H_{12}	44.24 %	51.22 %	10.40 %
Benzene, 1-ethyl-3-methyl-		C_9H_{12}	39.68 %	–	–
1H-Indene, 2,3-dihydro-5-methyl-	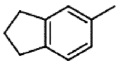	$C_{10}H_{12}$	16.08 %	–	–
1-Nonadecene		$C_{19}H_{38}$		3.65 %	
Total aromatics			100 %	96.35 %	99.10 %

to their 36 % reduction in friction and 76 % reduction in the wear rate (Table 2). The presence of tribofilm was further identified with Raman spectra. Fig. 15(a) represents the Raman spectra for weartracks with PO and PO-2 %IL samples. It was observed that for only PO, no distinguishable peak was visible whereas for PO-2 %IL, significant peaks around 1200, 1375, and 1600 cm^{-1} were observed representing sulfonic acid, aromatic azo, and amide groups [42]. It indicates that the IL exhibited chemical reactions with PO at the surface that provided sulfonic acid and amide from sulfonamide (functional group in saccharinate). The presence of sulfonic acid, aromatics and amide groups in the interface protected the surface from friction and wear than base PO [43,44].

The influence of tribofilm was also evident in case of LPO-A-2 %IL, where the LPO-A already contained double aromatic ring structure. The 2 % addition of IL in LPO-A reduced the friction by 26 % and the wear by 28 % (Table 3) which could be attributed to the formation of the reactive tribofilm. As a result, the formation of iron oxide was restricted to some extent. Fig. 15(b) shows the Raman spectra of LPO-A-2 %IL wear track, where it is observed that the peak intensity corresponding to iron oxides reduced in 2 % IL, whereas an additional peak around 2400 cm^{-1} indicates the presence of P-H group, probably coming out of Phosphine oxides (H_3PO), which ensures the presence of phosphorus on the wear track [45]. Thus, the presence of phosphorus in the cationic moiety of [P6,6,6,14][Sacc] PRTIL, helped in reducing the friction and wear by offering a P-rich tribofilm at the interface. Therefore, [P6,6,6,14][Sacc] worked as an efficient anti-wear and anti-friction additive for the plastic derived oil.

While it is evident that 2 % IL additive efficiently reduced the COF and wear for PO; there is scope to further improve the performance by optimizing the additive concentration, through the usage of machine learning models. For instance, in the recent literature, Wen et al. [46] proposed an eXtreme Gradient Boosting machine learning method to predict the tribological performance of lubricant, where Partical swarm optimization computational technique was used to optimize the additive concentration. Besides, Hasan et al. [47] used Gradient Boosting Machine (GBM), Random Forest (RF), K-Nearest Neighbor (KNN), and RF-GBM hybrid regression models to correlate friction, wear and material properties that satisfactorily could predict the COF and wear of aluminum-graphite composites. Similar algorithms may be useful to predict COF and wear for PO-IL blends on different surfaces. Such studies could potentially unlock the hidden possibilities of PO-IL blends for machine lubrication in the future.

5. Lubrication mechanism

Based on the above discussions, the possible lubrication mechanism for ILs incorporated with base oil samples is shown in Fig. 16. Three important factors that contributed to the tribological improvements were: (i) physicochemistry, (ii) chemical structure, and (iii) interfacial properties.

The viscosity of the blends increased with added percentage of IL, and that increased the film thickness. The ionic conductivity of base oil-IL blends helped in ionic dissociation and micelle formation which worked as a separator between asperities and provided better protection compared to base plastic derived oil. The presence of aromatic structure enhanced the adsorption capability of the oil and reduced asperity-asperity interaction, to reduce friction and wear. Lastly, the active elements such as P, S was able to create reactive tribofilm that enhanced the protection against friction and wear. Considering all these facts, it could be concluded that plastic pyrolysis oils containing aromatic structures could be utilized as useful lubricants, and their tribological performance could be further enhanced with incorporating bio-based ILs.

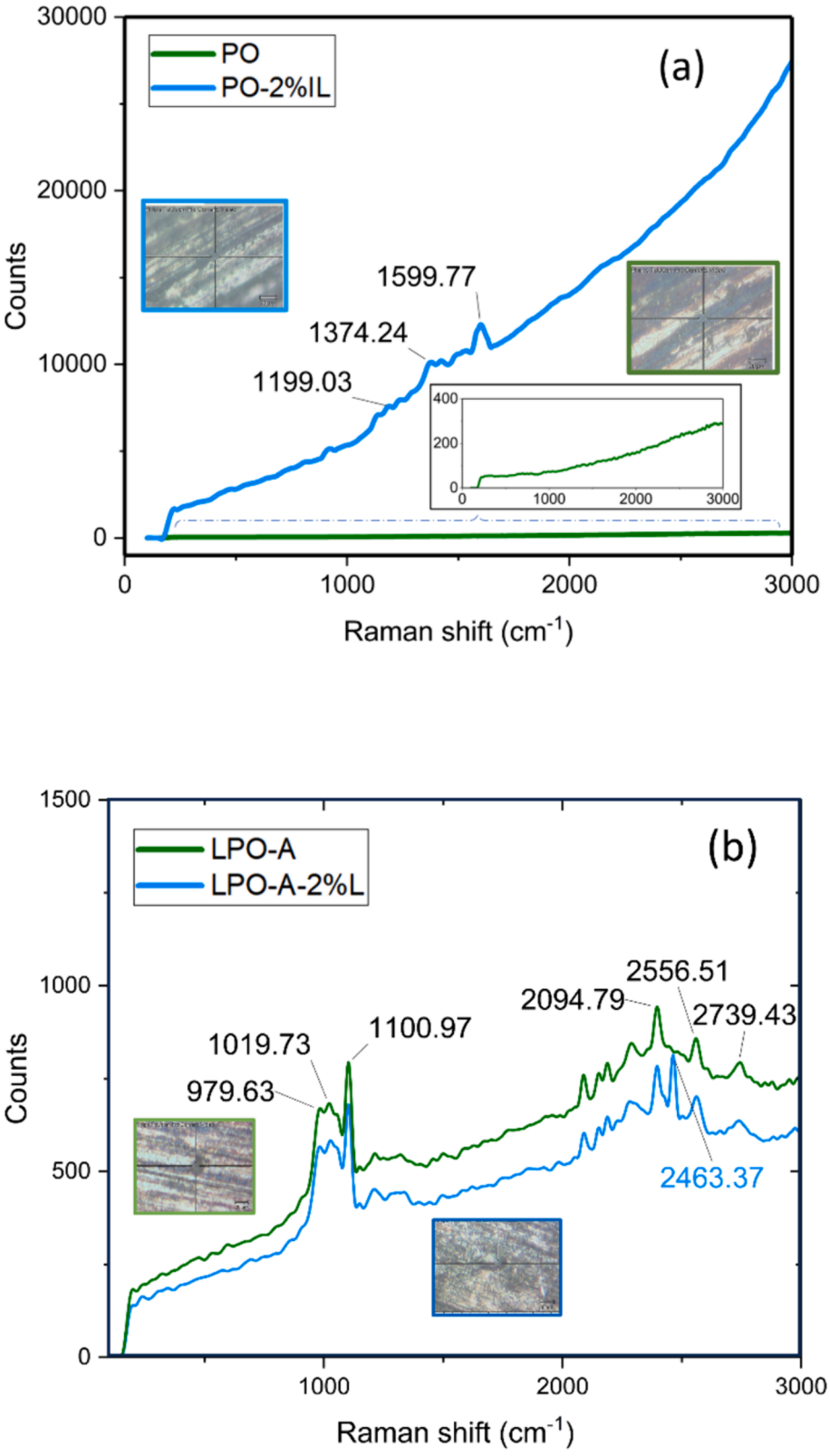

Fig. 15. Raman spectra for the worn surfaces with (a) PO and PO-2 %IL, (b) LPO-A and LPO-A-2 %IL samples.

6. Conclusions

Current study provided the experimental evidence of possible improvement pathway for plastic derived oil tribology. Using proper experimental conditions (temperature, reactor, catalyst type and loading) the presence of aromatic ring in the plastic derived oil can be ensured which will reduce the COF and wear rate significantly. The important conclusions that can be drawn from this research are as follows:

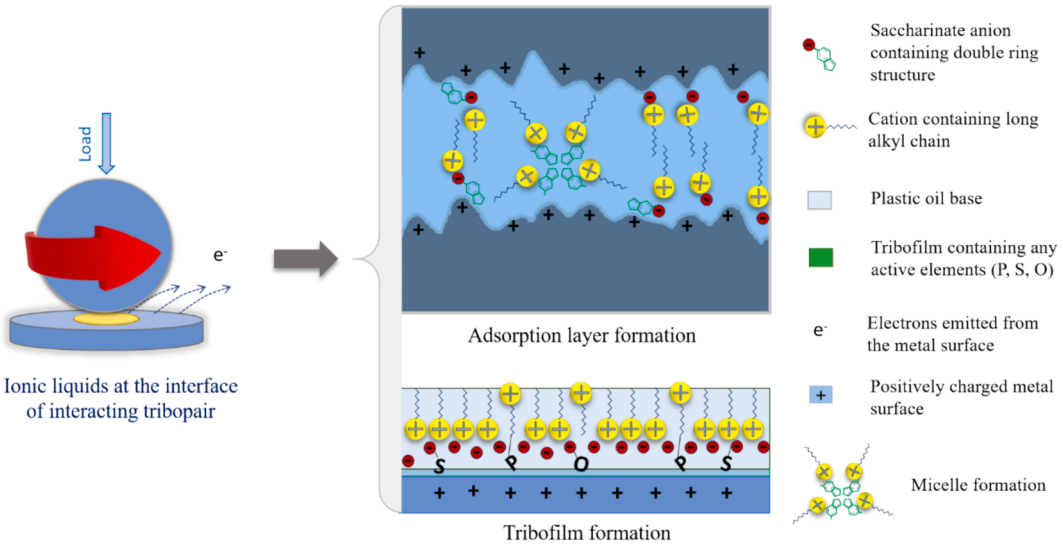

Fig. 16. Lubrication mechanism for PO-IL blends.

- Through adding 1 %, 2 % and 5 % IL into base PO, the COF was reduced by 29 %, 36 %, and 49 %, and the wear rate was reduced by 36 %, 76 %, and 81 % respectively.
- For LPO-A, LPO-B and LPO-C, the 2 % IL reduced COF by 26 %, 17 %, and 50 %, whereas wear rate was reduced by 28 %, 73 %, and 75 % respectively.
- The presence of aromatic double ring structure improved the tribological performance of plastic derived oil. Also, the presence of both aliphatic and aromatic structures in IL additive significantly helped in the tribological improvements.
- IL additive improved the viscosity, and film thickness of plastic derived oil. IL improved the cohesion interaction of PO which helped in providing a stable film reducing friction and wear for plastic derived oils.
- Ionic dissociation of IL in plastic derived oil helped in micelle formation which has played a role in the tribological improvement of plastic derived oil samples.
- The tribochemical film formed due to the additive shows the presence of P and S which could have provided enhanced protection against friction and wear.
- Bio-based [P6,6,6,14][Sacc] could be utilized as a novel additive to plastic derived oil to improve its tribological performance.

Overall, the incorporation of saccharinate based PRTIL in plastic derived oil could lead to a novel direction for the future studies in this area. As such, this research can play a crucial role in navigating the plastic derived oil tribology research for a sustainable future.

CRediT authorship contribution statement

Md Hafizur Rahman: Writing – review & editing, Writing – original draft, Visualization, Methodology, Investigation, Formal analysis, Data curation, Conceptualization. **Soumya Sikdar:** Writing – review & editing, Investigation. **Prakashbhai R. Bhoi:** Writing – review & editing, Supervision, Conceptualization. **Pradeep L. Menezes:** Writing – review & editing, Supervision.

Declaration of competing interest

The authors declare that they have no known competing financial interests or personal relationships that could have appeared to influence the work reported in this paper.

Data availability

Data will be made available on request.

Acknowledgement

The authors appreciate the financial support of the National Science Foundation, USA (Grant No. CMMI-2010205) and the laboratory facility of the Department of Mechanical Engineering, at the University of Nevada-Reno for ionic liquid-based lubricant formulation, property evaluation, and tribotesting. Additionally, the authors want to acknowledge the research facility and support provided by the Allen E. Paulson College of Engineering at Georgia Southern University for obtaining and testing the lab-scale pyrolysis oil. We also thank Tataianna Macias for assisting with a few viscosity and density measurements.

References

[1] L. Neufeld, F. Stassen, R. Sheppard, T. Gilman, The new plastics economy: rethinking the future of plastics, World Economic Forum, 2016. Access date: 15 May, 2024. https://www.ellenmacarthurfoundation.org/the-new-plastics-economy-rethinking-the-future-of-plastics.
[2] E.V. Deutschland, M. Düsseldorf, Plastics – the facts 2019 an analysis of European plastics: production, demand and waste data, Plastics Europe, 2019. Access date: 15 May, 2024. https://www.plasticseurope.org/application/files/1115/7236/4388/FINAL_web_version_Plastics_the_facts2019_14102019.pdf.
[3] M.H. Rahman, P.R. Bhoi, An overview of non-biodegradable bioplastics, J. Clean. Prod. (2021) 126218, https://doi.org/10.1016/j.jclepro.2021.126218.
[4] R. Geyer, J.R. Jambeck, K.L. Law, Production, use, and fate of all plastics ever made, Sci. Adv. 3 (2017) e1700782.
[5] K. Holmberg, A. Erdemir, Influence of tribology on global energy consumption, costs and emissions, Friction 5 (2017) 263, https://doi.org/10.1007/s40544-017-0183-5.
[6] Prakashbhai Bhoi, M.H. Rahman, Hydrocarbons recovery through catalytic pyrolysis of compostable and recyclable waste plastics using a novel desk-top staged reactor, Environ. Technol. Innov. 27 (2022) 102453, https://doi.org/10.1016/j.eti.2022.102453.
[7] M.H. Rahman, P.R. Bhoi, P.L. Menezes, Pyrolysis of waste plastics into fuels and chemicals: a review, Renew. Sustain. Energy Rev. 188 (2023) 113799, https://doi.org/10.1016/j.rser.2023.113799.
[8] A. Al-Rumaihi, M. Shahbaz, G. Mckay, H. Mackey, T. Al-Ansari, A review of pyrolysis technologies and feedstock: a blending approach for plastic and biomass towards optimum biochar yield, Renew. Sustain. Energy Rev. 167 (2022) 112715, https://doi.org/10.1016/j.rser.2022.112715.
[9] S. Sikdar, A. Siddaiah, P.L. Menezes, Conversion of waste plastic to oils for tribological applications, Lubricants 8 (2020) 78, https://doi.org/10.3390/lubricants8080078.
[10] R.A. Hackler, K. Vyavhare, R.M. Kennedy, G. Celik, U. Kanbur, P.J. Griffin, A. D. Sadow, G. Zang, A. Elgowainy, P. Sun, Synthetic lubricants derived from plastic

waste and their tribological performance, ChemSusChem 14 (2021) 4181, https://doi.org/10.1002/cssc.202100912.
[11] V. Cappello, P. Sun, G. Zang, S. Kumar, R. Hackler, H.E. Delgado, A. Elgowainy, M. Delferro, T. Krause, Conversion of plastic waste into high-value lubricants: techno-economic analysis and life cycle assessment, Green Chem. 24 (2022) 6306, https://doi.org/10.1039/D2GC01840C.
[12] S. Sikdar, M.H. Rahman, A.M. Ralls, P.L. Menezes, Enhancement in tribological performance of plastic oil by solid lubricant additives, Lubr. Sci. (2023) 420, https://doi.org/10.1002/ls.1647.
[13] M.H. Rahman, A. Khajeh, P. Panwar, M. Patel, A. Martini, P.L. Menezes, Recent progress on phosphonium-based room temperature ionic liquids: Synthesis, properties, tribological performances and applications, Tribol. Int. 167 (2022) 107331, https://doi.org/10.1016/j.triboint.2021.107331.
[14] C.J. Reeves, A. Siddaiah, P.L. Menezes, Friction and wear behavior of environmentally friendly ionic liquids for sustainability of biolubricants, J. Tribol. 141 (2019) 051604, https://doi.org/10.1115/1.4042872.
[15] C.J. Reeves, A. Siddaiah, P.L. Menezes, Tribological study of imidazolium and phosphonium ionic liquid-based lubricants as additives in carboxylic acid-based natural oil: advancements in environmentally friendly lubricants, J. Clean. Prod. 176 (2018) 241, https://doi.org/10.1016/j.jclepro.2017.12.099.
[16] C.J. Reeves, A. Siddaiah, P.L. Menezes, Ionic liquids: a plausible future of bio-lubricants, J. Bio-and Tribo-Corrosion 3 (2017) 1, https://doi.org/10.1007/s40735-017-0076-1.
[17] H. Xiao, Ionic liquid lubricants: basics and applications, Tribol. Trans. 60 (2017) 20, https://doi.org/10.1080/10402004.2016.1142629.
[18] I. Minami, T. Inada, R. Sasaki, H. Nanao, Tribo-chemistry of phosphonium-derived ionic liquids, Tribol. Lett. 40 (2010) 225, https://doi.org/10.1007/s11249-010-9626-0.
[19] J. Viesca, M. Mallada, D. Blanco, A. Fernández-González, J. Espina-Casado, R. González, A.H. Battez, Lubrication performance of an ammonium cation-based ionic liquid used as an additive in a polar oil, Tribol. Int. 116 (2017) 422, https://doi.org/10.1016/j.triboint.2017.08.004.
[20] D.W. Johnson, The tribology and chemistry of phosphorus containing lubricant additives, Adv. Tribol. (2016) 175, https://doi.org/10.5772/62208.
[21] C.J. Reeves, A.K. Kasar, P.L. Menezes, Tribological performance of environmental friendly ionic liquids for high-temperature applications, J. Clean. Prod. (2021) 123666, https://doi.org/10.1016/j.jclepro.2020.123666.
[22] M.H. Rahman, T. Liu, T. Macias, M. Misra, M. Patel, A. Martini, P.L. Menezes, Physicochemical and tribological comparison of bio-and halogen-based ionic liquid lubricants, J. Mol. Liq. 369 (2023) 120918, https://doi.org/10.1016/j.molliq.2022.120918.
[23] M.H. Rahman, P.R. Bhoi, A. Saha, V. Patil, S. Adhikari, Thermo-catalytic co-pyrolysis of biomass and high-density polyethylene for improving the yield and quality of pyrolysis liquid, Energy 225 (2021) 120231, https://doi.org/10.1016/j.energy.2021.120231.
[24] ARC, Quantification with the Polyarc, Activated Research Company (ARC), 2020. Access date: 15 May, 2024. https://www.activatedresearch.com/polyarc-universal-gc-fid-response/.
[25] B.J. Hamrock, D. Dowson, in: Ball Bearing Lubrication: The Elastohydrodynamics of Elliptical Contacts, ASME, New York, NY, USA, 1981, pp. 279–281, https://doi.org/10.1115/1.3253193.
[26] G.W. Stachowiak, A.W. Batchelor, Engineering tribology, Butterworth-Heinemann (2000).
[27] P.L. Menezes, S.V. Kailas, Effect of roughness parameter and grinding angle on coefficient of friction when sliding of Al–Mg alloy over EN8 steel, J. Tribol. 128 (4) (2006) 697, https://doi.org/10.1115/1.2345401.
[28] M.H. Rahman, A. Martini, P.L. Menezes, Relationship between structure and properties of bio-based aromatic ionic liquids for tribological applications, 2024, Available at SSRN 4933180. https://doi.org/10.2139/ssrn.4933180.
[29] S. Sikdar, P.L. Menezes, Enhancing lubrication performance of plastic oil lubricant with oleic acid-functionalized graphene nanoplatelets and hexagonal boron nitride solid lubricant additives, Lubricants 12 (2024) 251, https://doi.org/10.3390/lubricants12070251.
[30] A.K. Kasar, M.H. Rahman, B. D'Souza, P.L. Menezes, Tribological performance of ionic liquid impregnated porous aluminum borate ceramic, Tribol. Int. 180 (2023) 108219.
[31] L.D. Aguilera-Camacho, M.T. Hernández-Sierra, J.S. García-Miranda, K.J. Moreno, On the influence of tribological properties of AISI 4140 annealed steel against ceramic counterparts under dry and lubricated conditions and their effect on steel microstructure, Metals 11 (2021) 1275, https://doi.org/10.3390/met11081275.
[32] K. Bearings, Bearing Ball Materials, 2021. Access date: 15 May, 2024. https://www.kmsbearings.com/materials/ball-bearing-materials.html.
[33] C.A. Angell, Y. Ansari, Z. Zhao, Ionic liquids: past, present and future, Faraday Discuss. 154 (2012) 9, https://doi.org/10.1039/C1FD00112D.
[34] P. Jain, A. Kumar, Comparable ionicity of the solutions of aprotic and protic ionic liquids by anion substitution, J. Solution Chem. 46 (2017) 1315, https://doi.org/10.1007/s10953-017-0640-9.
[35] W. Silva, M. Zanatta, A.S. Ferreira, M.C. Corvo, E.J. Cabrita, Revisiting ionic liquid structure-property relationship: a critical analysis, Int. J. Mol. Sci. 21 (2020) 7745. https://www.mdpi.com/1422-0067/21/20/7745.
[36] M. Cai, Q. Yu, W. Liu, F. Zhou, Ionic liquid lubricants: when chemistry meets tribology, Chem. Soc. Rev. (2020) 7753, https://doi.org/10.1039/D0CS00126K.
[37] P. Pandey, A.E. Somers, S.K. Hait, M. Forsyth, S. Ramakumar, A novel approach to improve the oil miscibility and incorporate multifunctionality in ionic liquids as lubricant additives, PCCP 23 (2021) 3429, https://doi.org/10.1039/D0CP05295G.
[38] S.L. Garvey, The University of Wisconsin-Milwaukee, 2013. https://dc.uwm.edu/etd/100.
[39] K. Birdi, in: Handbook of Surface and Colloid Chemistry, CRC Press, 2008, https://doi.org/10.1201/b18633.
[40] P. Sharma, S. Sharma, H. Kumar, Introduction to ionic liquids, applications and micellization behaviour in presence of different additives, J. Mol. Liq. (2023) 123447, https://doi.org/10.1016/j.molliq.2023.123447.
[41] J. Appeldoorn, F. Tao, The lubricity characteristics of heavy aromatics, Wear 12 (1968) 117, https://doi.org/10.1016/0043-1648(68)90339-6.
[42] U.O.C. Irvine, RAMAN Band Correlation Table, 2024. Access date: 15 May, 2024. https://www.chem.uci.edu/~dmitryf/manuals/Raman%20correlations.pdf.
[43] Y. Shitara, A. Kanno, T. Kaimai, S. Mori, Effect of amide molecular structure on tribological properties of thermoreversible gel lubricant, Tribology Online 5 (2010) 284, https://doi.org/10.2474/trol.5.284.
[44] H. Lei, W. Guan, J. Luo, Tribological behavior of fullerene–styrene sulfonic acid copolymer as water-based lubricant additive, Wear 252 (2002) 345, https://doi.org/10.1016/S0043-1648(01)00888-2.
[45] K.D. Troev, Reactivity of PH Group of Phosphorus Based Compounds, Academic Press, 2017 https://www.sciencedirect.com/book/9780128138342/reactivity-of-p-h-group-of-phosphorus-based-compounds.
[46] G. Wen, W. Liu, X. Wen, P. Wei, H. Cao, P. Bai, Y. Tian, Effective tribological performance-oriented concentration optimization of lubricant additives based on a machine learning approach, Tribol. Int. 197 (2024) 109770, https://doi.org/10.1016/j.triboint.2024.109770.
[47] M.S. Hasan, A. Kordijazi, P.K. Rohatgi, M. Nosonovsky, Machine learning models of the transition from solid to liquid lubricated friction and wear in aluminum-graphite composites, Tribol. Int. 165 (2022) 107326, https://doi.org/10.1016/j.triboint.2021.107326.